Effect of quench depth on grain structure in quiescently ordered block copolymers

W. G. Kim, M. Y. Chang, B. A. Garetz,[a] and M. C. Newstein
Departments of Physics, Chemical Engineering, Chemistry, and Materials Science, and Electrical Engineering, Polytechnic University, Brooklyn, New York 11201

N. P. Balsara,[b] J. H. Lee, and H. Hahn
Department of Chemical Engineering, University of California, Berkeley, California 94720

S. S. Patel
Bell Laboratories, Lucent Technologies, Murray Hill, New Jersey 07974

(Received 28 August 2000; accepted 31 January 2001)

Grain growth in a polystyrene–polyisoprene block copolymer melt is studied by time-resolved depolarized light scattering after a quiescent quench from the disordered to the ordered state. At shallow quench depths, classical nucleation and growth kinetics are observed. Grains comprising the equilibrated ordered phase nucleate and grow by consuming the surrounding disordered phase. In contrast, deep quenches result in the formation of disorganized grains with an average order parameter that is well below the equilibrium value. Small angle neutron scattering and rheological experiments were conducted to facilitate the interpretation of the light scattering data. We show that the nonequilibrium grain structure formed during deep quenches is due to extremely high nucleation density. Under these circumstances, the space required for the formation of equilibrated grains is unavailable. © *2001 American Institute of Physics.* [DOI: 10.1063/1.1357796]

I. INTRODUCTION

Ordered crystalline and liquid crystalline phases formed in the absence of external fields contain numerous defects.[1–5] Coherent order is restricted to regions called grains. Manipulating grain structure to obtain the desired material properties is common practice. Some applications require materials with high defect density while others require complete elimination of defects. The grain structure in a given sample is determined by processing history. Shallow quenches from the liquid state produce large grains while deep quenches produce small grains. Coherent order can be suppressed completely if the cooling is rapid enough, resulting in vitrification or glass formation. A unified framework for quantifying the processes that are responsible for grain structure and vitrification in different materials has not yet been developed. This is because grain structure is determined by a complex interplay between thermodynamic and kinetic factors. Consequently, processes leading to the desired grain structure are identified empirically. The mechanical properties of liquid crystalline grains are highly anisotropic; viscous flow is obtained along the liquid axes while solidlike elasticity is obtained along the other axes. This attribute introduces further complications in the relationship between quenching conditions and grain structure. It is thus not surprising that many questions about the factors that control grain structure in liquid crystals remain unresolved.

Our objective is to identify the thermodynamic and kinetic factors that govern grain structure in a hexagonal liquid crystal system. We study a polystyrene–polyisoprene block copolymer melt which forms an ordered phase consisting of polyisoprene cylinders arranged on a hexagonal lattice, embedded in a polystyrene matrix.[6] The birefringence of ordered block copolymers Δn (the difference in refractive index for light polarized parallel and perpendicular to the cylinder axes) is about 10^{-4}. The material is highly transparent in both the ordered and disordered state and grain formation can be conveniently studied by depolarized light scattering. We performed additional small angle neutron scattering (SANS) and rheological experiments to facilitate the interpretation of the light scattering data.

This paper is part of a series wherein block copolymer grain structure is probed by depolarized light scattering.[7–14] The present experimental system was designed to cover a much wider range of quenching conditions than the previous experiments. We found that changing the system led to new and unexpected results. The main purpose of this paper is to report these findings.

The grain structure of block copolymers has been probed by a variety of other techniques. The topology of defects such as wedge and screw dislocations were studied by transmission electron microscopy (TEM).[15,16] A comparison of grain structure determined by TEM and depolarized light scattering has been conducted.[9] Defect annihilation processes in block copolymer thin films have been studied by direct imaging techniques such as atomic force microscopy (AFM).[17–19] In some systems, the grain structure can be inferred from ultra low angle x-ray scattering experiments.[20]

[a]Author to whom correspondence should be addressed. Electronic mail: bgaretz@duke.poly.edu
[b]Author to whom correspondence should be addressed. Electronic mail: nbalsara@cchem.berkeley.edu

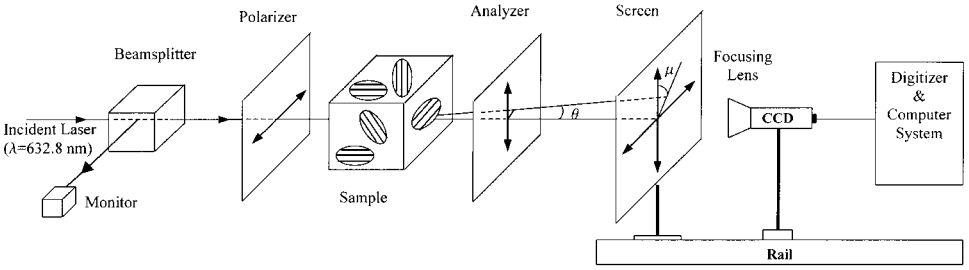

FIG. 1. Schematic of depolarized light scattering apparatus and definition of scattering geometry.

II. MATERIALS, INSTRUMENTATION, AND DATA ACQUISITION

A polystyrene–polyisoprene diblock copolymer was synthesized by anionic polymerization under high vacuum, using methods described elsewhere.[21] The weight average molar masses of the polystyrene and polyisoprene blocks were determined to be 19.8 and 6.0 kg/mol, respectively, and the polydispersity index of the copolymer was 1.07. We refer to this polymer as SI(20-6). The polymer characterization procedures are given in Ref. 21. About 0.5 wt. % BHT (2,6-di-tert-butyl-4-methylphenol) was added to a benzene solution of the polymer to prevent oxidative degradation. The polymer was isolated by freeze-drying and stored in a freezer at $-11\,^{\circ}\mathrm{C}$.

The order–disorder transition temperature, T_{ODT}, of SI(20-6) was determined by the birefringence method[22,23] and found to be $133\pm1\,^{\circ}\mathrm{C}$. The volume fraction of polyisoprene in the block copolymer is 0.26. Based on extensive characterization of polystyrene–polyisoprene block copolymers,[24] we expect the sample to have a cylindrical microstructure at temperatures of interest, $116\,^{\circ}\mathrm{C}$–$132\,^{\circ}\mathrm{C}$. The glass transition temperature of the polystyrene-rich microphase was measured by differential scanning calorimetric experiments conducted on an ordered sample and determined to be $78\,^{\circ}\mathrm{C}$. The glass transition was seen more clearly during cooling than heating; both experiments were conducted at $10\,^{\circ}\mathrm{C}$/min. Our studies on order formation were thus conducted well above the glass transition temperature of the polystyrene-rich microphase.

The light scattering experiments were conducted on 1 mm thick SI(20-6) melts enclosed between optical flats. The samples were made by placing the appropriate amount of polymer on a 1 mm thick optical flat. A black anodized aluminum spacer with an inner diameter of 16 mm was placed around the polymer. The assembly comprising the spacer, quartz disk, and polymer were heated to $150\,^{\circ}\mathrm{C}$ in a vacuum oven until a bubble-free polymer sample was obtained. The polymer was then capped by a second optical flat in nitrogen atmosphere and the cell was sealed with a high temperature glue.

The depolarized light scattering experiments were conducted on a homebuilt apparatus described in Ref. 11. A schematic of the light scattering experiment is shown in Fig. 1. A beam of light from a 15 mW He–Ne laser with $\lambda=633\,\mathrm{nm}$ was used as the source. A beamsplitter was used to direct a small portion (5%) of the laser output onto a photodiode. The photodiode reading was used to monitor changes in the incident beam; we refer to this as the monitor photodiode. The main beam was directed through a horizontal polarizer, and a quarter-wave plate, which was used as a compensator. The light emerging from the sample passed through an analyzer whose optic axis was perpendicular to the polarizer and was projected onto a screen. A charge coupled device (CCD) camera equipped with a focusing lens was used to capture the two-dimensional scattering data projected onto the screen. The scattering intensity was recorded as a function of scattering angle θ along 2 azimuthal angles, $\mu=0^{\circ}$ and $\mu=45^{\circ}$ (see Fig. 1). Before each experiment, the sample was disordered by heating to $142\,^{\circ}\mathrm{C}$ for 40 min, to ensure a uniform starting condition for all of the experiments. The depolarized light scattering signal in the disordered state was measured, and taken to be the background signal. The sample was then quenched into the ordered state and the depolarized light scattering intensity profiles were measured as a function of time. Time zero ($t=0$) is defined as the time at which the set point on the temperature controller was changed. It took between 32 and 42 min for the sample temperature to reach within $1\,^{\circ}\mathrm{C}$ of the final quench temperature; the deepest quench ($116\,^{\circ}\mathrm{C}$) required 42 min while the shallowest quench ($130\,^{\circ}\mathrm{C}$) required 32 min. The time-dependent depolarized light scattering profiles were measured for a minimum of 3 h($t=180\,\mathrm{min}$).

Details regarding the conversion of the raw data to depolarized scattering intensity $I(q,\mu)$ are very similar to those given in Ref. 11. The only difference is that the measured intensity in the present experiments was normalized by the monitor photodiode signal to account for changes in the incident intensity. In some experiments, the scattering signal exceeded the saturation limit of our CCD camera. In such cases, a neutral density filter, with a nominal transmission coefficient of 0.1, was introduced into the optical path with the help of a translation stage, before the beamsplitter. The neutral density filter is not shown in Fig. 1 for clarity. The normalization of the scattering profiles using the monitor signal described above accounts for the presence of the neutral density filter and drifts in the laser intensity. In some ordered samples we found a bright central spot that could not be extinguished by rotating the compensator and polarizers. The bright spot may be due to nonrandomness in the grain organization or residual stresses due to the solidlike character of the ordered phase. In cases where a bright spot was obtained, the scattering signal within the bright spot was ignored. The depolarized light scattering intensity I along $\mu=0^{\circ}$ and 45° is reported as a function of the scattering vector q, [$q=4\pi\sin(\theta/2)/\lambda$, where θ is the scattering angle and λ is the

wavelength of the incident light beam], after monitor and background corrections.

The scattering data from a finite collection of grains contains speckles due to constructive and destructive interference from particular pairs of widely separated grains. The scattering equations that we will develop in the next section apply to averages over such speckled patterns from statistically equivalent samples. In systems with rapid dynamics (e.g., dilute polymer solutions), one can obtain averaged data by time averaging. However, the dynamical processes in ordered block copolymers are extremely slow. In such samples, one can obtain averages by translating or rotating the sample. However, we found that the grain structure in our samples is affected by motion, presumably due to the flow-aligning character of block copolymers. We thus obtain averaged $I(q,\mu)$ by averaging the measured scattering data in four adjacent pixels in the CCD camera, along the specified direction μ.

SANS experiments were conducted on the NG3 beamline at the National Institute of Standards and Technology in Gaithersburg, Maryland, using the following configuration: neutron wavelength, $\lambda = 6.0$ Å, wavelength spread, $\Delta\lambda/\lambda = 0.15$, sample-to-detector distance $= 4$ m, sample aperture $= 0.635$ cm, source-to-sample distance $= 5.47$ m, and source size $= 5.0$ cm. The scattering data were collected using a two-dimensional detector, corrected for background scattering, empty cell scattering, and detector sensitivity. We report the azimuthally averaged scattering intensity as a function of q (same definition as above except that λ is the wavelength of the incident neutron beam). The raw data were converted to absolute coherent scattering intensity, $I_{\mathrm{SANS}}(q)$, using methods and secondary standards described in Ref. 21.

Rheological measurements were conducted on an ARES instrument built by Rheometrics Scientific in a dry nitrogen environment, using 25 mm diam parallel plate fixtures, and a transducer with a dynamic range between 200 and 0.2 g cm. The location of the point of contact between the parallel plates was noted. The lower plate was detached and 3 g of the polymer was placed on the plate. A retaining ring around the plate was used to keep the polymer from flowing off the plate. The assembly of the lower plate, retaining ring, and polymer were placed in a vacuum oven at 150 °C until a bubble-free sample was obtained. After cooling to room temperature, the lower plate with the polymer sample was reattached to the rheometer. The upper plate was then lowered at 150 °C in the ARES oven under dry nitrogen to yield a 1.5 mm thick sample.

III. THEORETICAL MODEL FOR INTERPRETATION OF DEPOLARIZED LIGHT SCATTERING DATA

We provide a brief summary of the equations that describe depolarized light scattering from ordered block copolymers. The model used in this work was developed in Ref. 14. We assume that the sample is composed of randomly oriented ordered grains coexisting with disordered regions. The volume fraction of the ordered grains is ϕ. Each grain is a birefringent, uniaxial crystal with optic axis parallel to the cylinder axis. The scattered field from this collection of grains is determined by the probability that given a point inside a grain with optic axis along a unit vector **g**, a vector **R** emanating from that point lies entirely within that grain. We assume that this probability distribution $C(\mathbf{R},\mathbf{g})$ is of the Gaussian-ellipsoidal form,

$$C(\mathbf{R},\mathbf{g}) = \exp\left[-\frac{1}{2}\left(\frac{\mathbf{a}\cdot\mathbf{R}}{w}\right)^2\right]\exp\left[-\frac{1}{2}\left(\frac{\mathbf{b}\cdot\mathbf{R}}{w}\right)^2\right] \times \exp\left[-\frac{1}{2}\left(\frac{\mathbf{g}\cdot\mathbf{R}}{l}\right)^2\right], \tag{1}$$

where $\{\mathbf{g},\mathbf{a},\mathbf{b}\}$ are an orthogonal set of unit vectors. The characteristic lengths of the ellipsoidal grains in the directions parallel and perpendicular to the optic axis are l and w, respectively. The scattering profiles, $I(q,\mu)$ for such a system along the $\mu = 0°$ and 45° directions is given by

$$I(q,0°) = I_0[C(q) + D(q)] \tag{2}$$

and

$$I(q,45°) = I_0[C(q) - D(q)], \tag{3}$$

where

$$C(q) = \frac{15}{16}\exp\left(-\frac{q^2w^2}{2}\right)\int_0^{\pi} d\alpha \sin^5\alpha \times \exp[-\beta(\alpha)] I_{m0}[\beta(\alpha)] \tag{4}$$

and

$$D(q) = -\frac{15}{16}\exp\left(-\frac{q^2w^2}{2}\right)\int_0^{\pi} d\alpha \sin^5\alpha \times \exp[-\beta(\alpha)] I_{m2}[\beta(\alpha)], \tag{5}$$

$\beta(\alpha) = (q^2l^2/4)[1 - w^2/l^2]\sin^2\alpha$, I_{mj} is the modified Bessel function of order j, and

$$I_0 = K_c(\Delta n)^2 w^2 l \phi = K_c(\Delta n)^2 v \phi, \tag{6}$$

where K_c is an instrumental constant, and $v = w^2 l$ is the characteristic grain volume. The 15/16 factor in Eqs. (4) and (5) ensures that $\lim_{q\to 0} C(q) = 1$ [note that $\lim_{q\to 0} D(q) = 0$]. In previous papers,[11,14] this constant was absorbed into the definition of K_c.

For isotropic grains ($l = w$), $D(q) \equiv 0$ [see Eq. (5)], and Eqs. (2)–(4) reduce to a simple expression for $I(q,\mu)$ that is independent of μ,

$$I(q) = I_0 \exp\left(-\frac{q^2w^2}{2}\right) \quad \text{for } l = w \text{ only.} \tag{7}$$

IV. EFFECT OF QUENCH TEMPERATURE ON GRAIN STRUCTURE

A series of depolarized light scattering experiments were conducted where the sample was quenched from the disordered state to the ordered state. Each experiment was started by heating the sample to 142 °C, which is well above the order–disorder transition temperature for 40 min, followed by a quench to a predetermined temperature T in the ordered state. The results of these experiments are shown in Fig. 2 where we show the depolarized light scattering intensity obtained along $\mu = 45°$. In Fig. 2(a) we show results obtained

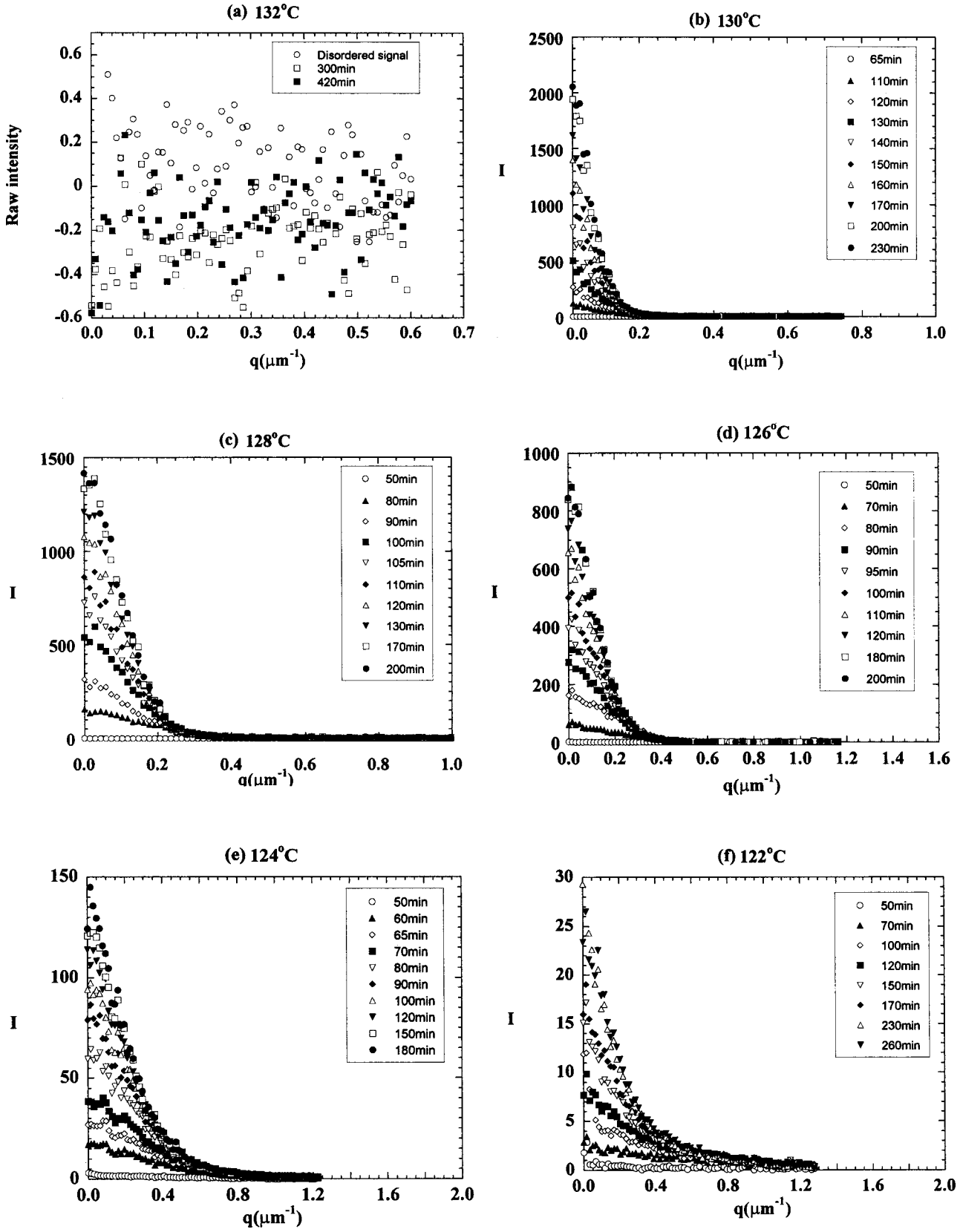

FIG. 2. Time dependent depolarized light scattering profiles along the $\mu = 45°$ direction after quenching from the disordered state to various temperatures below the order–disorder transition temperature (a) 132 °C. At this temperature we see no signs of the order formation and the uncorrected raw scattering data at $t = 420$ min are indistinguishable from that obtained in the disordered state prior to the quench. At all other quench temperatures we report the scattering intensity, I, after background and monitor corrections (see text for details); (b) 130 °C, (c) 128 °C, (d) 126 °C, (e) 124 °C, (f) 122 °C, (g) 120 °C, (h) 118 °C, (i) 116 °C.

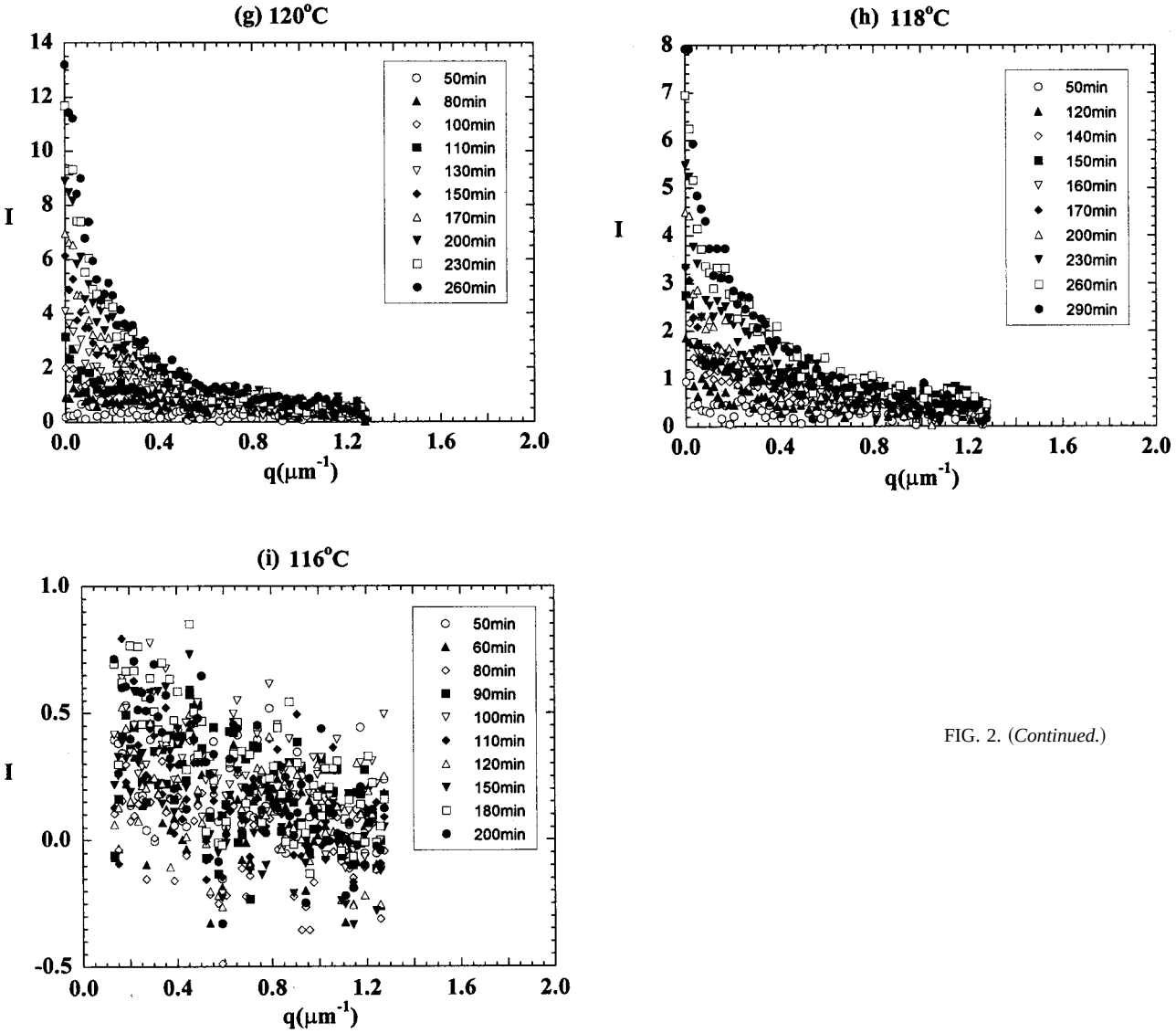

FIG. 2. (*Continued.*)

at $T=132\,^{\circ}\mathrm{C}$ which is just below T_{ODT}. We show raw scattering intensity obtained at $t=0$ which is the background signal, as well as data obtained at $t=300$ and 420 min. It is evident that there is no measurable change in the depolarized light scattering signal after quenching to 132 °C. We conclude that the thermodynamic driving force for order formation at 132 °C is too weak and we thus do not see any evidence of order formation on the experimental time scale. A dramatic difference is found when the sample is quenched to 130 °C; see Fig. 2(b). At this quench temperature (and most other temperatures discussed in this paper), the signal is well above the background. From this point forward we only discuss $I(q,\mu)$ after monitor and background corrections were made (see Sec. II). At $T=130\,^{\circ}\mathrm{C}$, the signal increases above the background at $t=65$ min and then continues to increase rapidly [Fig. 2(b)]. The scattering intensity at $q=0$ reaches 2000 units at $t=230$ min when the experiment was terminated. Note that the incident beam is not masked and thus I_0 (I at $q=0$) is obtained without resorting to extrapolation. We see clear signatures of the ordering process 3 °C below T_{ODT} [Fig. 2(b)] but not 1 °C below T_{ODT} [Fig. 2(a)]. Similar signatures were seen at lower quench temperatures as can be seen in Figs. 2(c)–2(i). However, the magnitude of the intensity obtained at the end of the experiment ($t\approx 200$ min) is a sensitive function of quench temperature. Changing the quench temperature from 130 °C to 116 °C leads to a monotonic reduction in I_0 from 2000 to 0.7. The fact that the depolarized light scattering signatures of order formation get weaker with increasing quench depth is somewhat surprising. At a quench temperature of 116 °C, the magnitude of the signal is comparable to the magnitude of the noise (0.5 units) at all stages of the experiment [see Fig. 2(i)]. This is an indication of extremely poor order. The data obtained at the shallowest and deepest quenches are thus quite similar [compare Figs. 2(a) and 2(i)].

At all times (when the scattering signal was well above the background), the profiles obtained at quench temperatures between 130 and 124 °C exhibited fourfold symmetry. Typical scattering data is shown in Fig. 3 where we show the raw data recorded on the CCD camera at $t=200$ min after quench from the disordered state to 128 °C. Figure 3 shows the two-dimensional data corresponding to the last data set shown in Fig. 2(c). The fourfold symmetry of the scattering

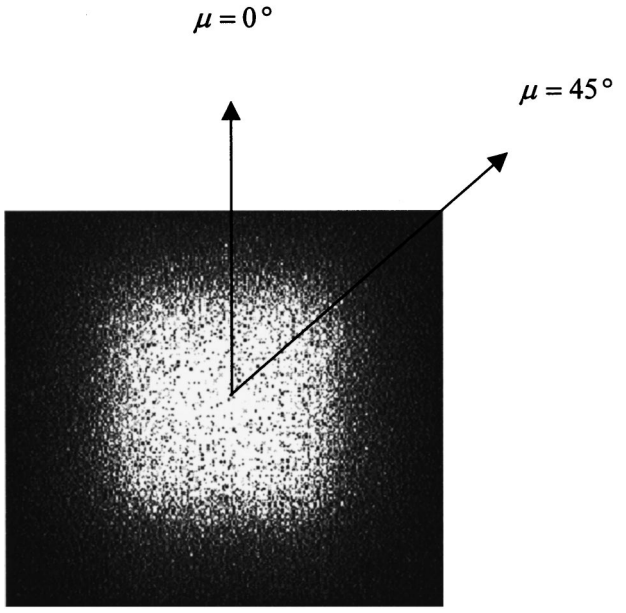

FIG. 3. Typical two-dimensional light scattering profiles obtained after shallow quenches. Data obtained at $t = 200$ min after quenching from the disordered state to 128 °C ($T_{ODT} = 133 \pm 1$ °C). The center of the main beam is located at the junction of the $\mu = 0°$ and $\mu = 45°$ rays.

pattern is clearly seen in Fig. 3. The scattering profiles $I(q)$ along $\mu = 0°$ and 45°, obtained from the two-dimensional data shown in Fig. 3, are shown in Fig. 4(a). It is evident that $I(q, \mu = 45°)$ is slightly larger than $I(q, \mu = 0°)$ in the range $0.05\,\mu\text{m}^{-1} < q < 0.25\,\mu\text{m}^{-1}$ range. At $q < 0.05\,\mu\text{m}^{-1}$, i.e., as $q \to 0$, the scattering intensity is independent of μ. This is consistent with Maxwell's equations, which require the electric field in the detector plane to be continuous at all points. At $q > 0.25\,\mu\text{m}^{-1}$ the scattering intensity is comparable to the background signal (the background is isotropic). The dashed and solid curves in Fig. 4(a) are fits of Eqs. (2) and (3) through the $\mu = 0°$ and 45° data, respectively, with l, w, and I_0 as adjustable parameters. The theoretical scattering curves were computed over a wide range of l, w, and I_0 values. The sum of the square of the deviation between the theoretical and experiment scattering intensity, $(\Delta I)^2$ over the entire range of q and μ were computed for each combination of l, w, and I_0. The combinations that gave the smallest average value of $|\Delta I|/I_0$ are reported in this paper. The theoretical curves in Fig. 4(a) correspond to $l = 17.3\,\mu$m, $w = 6.9\,\mu$m, and $I_0 = 1430$, and the corresponding average value of $|\Delta I|/I_0$ is 0.013.

The deviation between theory and experiment ($|\Delta I|/I_0$) decreased as the disorder-to-order transition progressed. In Fig. 4(b) we show data obtained at early times ($t = 55$ min). The curves in Fig. 4(b) represent least squares fits of our model as described in the preceding paragraph, which give $l = 7.5\,\mu$m, $w = 2.5\,\mu$m, and $I_0 = 2.2$. The corresponding value of $|\Delta I|/I_0$ is 0.045. The fact that error at $t = 55$ min $[(|\Delta I|/I_0)_{t=55\,\text{min}}]$ is 3 times larger than the error at $t = 200$ min $[(|\Delta I|/I_0)_{t=200\,\text{min}}]$ is not surprising because the signal to noise ratio at early times is small. Note that at $t = 50$ min, the signal is below the noise level.

It is evident from Figs. 4(a) and 4(b) that our model

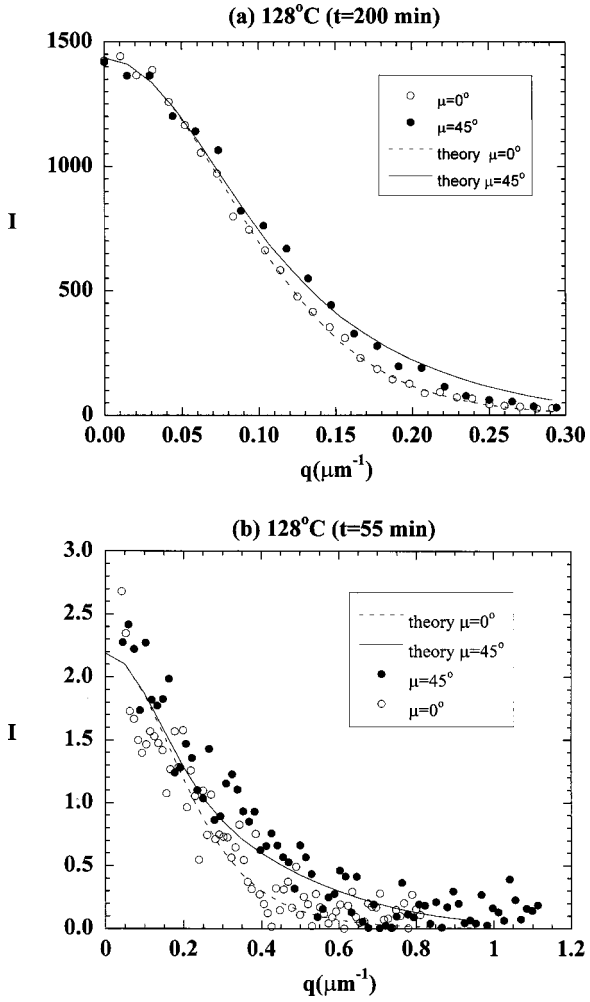

FIG. 4. Depolarized light scattering intensity along $\mu = 0°$ and 45° directions vs scattering vector q. The data were obtained after quenching from the disordered state to 128 °C. The curves are theoretical fits [Eqs. (2)–(5)] with l, w, and I_0 as adjustable parameters. (a) $t = 200$ min, (b) $t = 55$ min.

captures the essential features of our data. We analyzed all of the data obtained at quench temperatures between 130 and 124 °C using the ellipsoidal grain model because all of the data in this temperature range exhibited fourfold symmetry. Most of the $|\Delta I|/I_0$ values were in the 0.1–0.01 range; the only exceptions were the first recorded data set which, sometimes gave $|\Delta I|/I_0$ as high as 0.2. It is important to recognize that the grain structure of quiescently quenched block copolymers is extremely complex. Coherent order is interrupted by a variety of point, line, wall, and continuous (texture) defects. The values of l and w obtained from the analysis of the light scattering data should be interpreted as that average lengths over which coherence is obtained in the directions parallel and perpendicular to the optic axes, respectively. It is perhaps remarkable that a single model is consistent with all of the measured data, given the complexity of the grain structure being studied and the wide range of the grain parameters obtained. It should be noted that even in simple systems with a single correlation length, different functional forms are often needed to fit the low-q and high-q data.

At all times (when the scattering signal was well above the background), the profiles obtained at quench tempera-

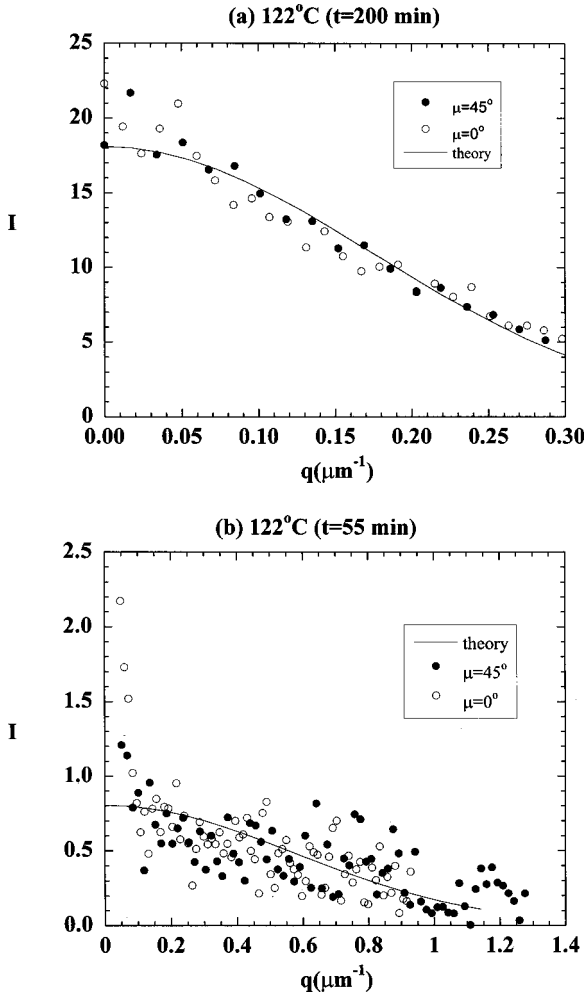

FIG. 5. Depolarized light scattering intensity along $\mu=0°$ and 45° directions vs scattering vector q. The data were obtained after quenching from the disordered state to 122 °C. The curves are theoretical fits [Eq. (7)] with w, and I_0 as adjustable parameters. (a) $t=200$ min, (b) $t=55$ min.

tures between 122 and 116 °C were azimuthally symmetric. An example of such data is shown in Fig. 5(a), where we show $I(q,\mu)$ obtained after quenching from the disordered state to 122 °C at $t=200$ min. Here we find that within experimental error, $I(q,0°)=I(q,45°)$. This indicates the presence of isotropic grains with $l=w$, and the scattering intensity profile is given by Eq. (7). In such cases the least squares fitting procedure described above was used on both sets of data ($\mu=0°$ and $\mu=45°$) with I_0 and w as adjustable parameters. The curve in Fig. 5(a) represents the least-squares fit through the data, giving $w=3.2\,\mu$m and $I_0=18.1$. We find reasonable agreement between the data and our model with $|\Delta I|/I_0=0.05$. The model underestimates the scattered intensity in the low q regime [see Fig. 5(a)]. Possible causes for this deviation between theory and experiment are discussed below. In Fig. 5(b) we show the scattering profile recorded during the early stages of the disorder-to-order transition at 122 °C ($t=55$ min) along with the least squares fit. Under these conditions we obtain $w=1.3\,\mu$m, $I_0=0.81$, and $|\Delta I|/I_0=0.1$. As mentioned in Sec. II, we ignore the spike in the data at $q\approx 0$, which corresponds to about 0.5% of the measured signal. The spike could be due to either a small number of very large grains, or a slight preferential orientation of the grains formed during the early stages of the disorder-to-order transition. It is evident that our single grain model is consistent with the data shown in Figs. 5(a) and 5(b). Similar consistency was obtained at all times at quench temperatures between 122 and 118 °C.

As seen in Figs. 4(a) and 4(b), the difference in scattering intensity along $\mu=0$ and 45° is relatively subtle and these differences can only be seen on an expanded scale (e.g., Fig. 4). On a more compact scale like that used in Fig. 2, there is no discernible difference in I vs q plots along $\mu=0$ and $\mu=45°$. For brevity, we therefore do not show plots of data obtained along $\mu=0°$. However, in all cases, the data obtained along $\mu=0$ was used in the analysis, as described in Sec. III. All of the data at quench temperatures between 130 °C and 124 °C were analyzed using Eqs. (2) and (3). All of the data at quench temperatures between 122 °C and 116 °C were analyzed using Eq. (7). We thus obtain the time dependence of l, w, and I_0 as a function of quench depth. Note that the same model is used for all of the data analysis, because the isotropic grain model is a special case of the ellipsoidal grain model. While our model captures the essential features of data obtained over a wide range of parameter space, it does not rule out the possibility of developing more accurate and appropriate models for describing the grain structure in block copolymers.

The time dependencies of l and w in the shallow quench regime, defined to be $124\,°\text{C}\leqslant T\leqslant 130\,°\text{C}$, are shown in Figs. 6(a) and 6(b), respectively. In Fig. 6 and in subsequent figures, a vertical gray bar is used to show the range of times required to change the temperature of the sample from the disordered to the ordered state (see Sec. II for details). At early times, l and w increase rapidly. At $T=130\,°\text{C}$, the shallowest quench where order formation was observed, we find that l reaches a maximum of 27 μm and then decreases with time [Fig. 6(a)], while w increases monotonically with time [Fig. 6(b)]. At the other temperatures in the shallow quench regime, l and w reach time-independent plateau values after $t\approx 150$ min; see Figs. 6(a) and 6(b). In Fig. 6(c) we show the time dependence of w in the deep quench regime, defined to be $116\,°\text{C}\leqslant T\leqslant 122\,°\text{C}$. In this regime the grains are isotropic and thus grains are characterized by one length scale w. At 122 °C [Fig. 6(c)], we see an increase in the grain size at early times followed by a plateau. This is similar to the trends seen in the shallow quench regime [Figs. 6(a) and 6(b)]. At 120 °C and 118 °C, however, the grain sizes increase continuously during the course of the experiment. The low signal to noise ratio at $T=116\,°\text{C}$ prevented us from obtaining reliable estimates of grain sizes during this quench [see Fig. 2(i)].

In Fig. 7 we show the time dependence of average grain volume, v ($v=lw^2$, or w^3 if $l=w$) for all of the quenches. We find that the time dependence of v is similar for all of the quenches. The grains are small during the early stages of the quench, grow rapidly at intermediate times ($50\text{ min}<t<150$ min), and then reach a plateau at long times ($t>150$ min). At the lowest quench depth ($T=130\,°\text{C}$), the grain structure (l and w) continues to evolve at $t>150$ min

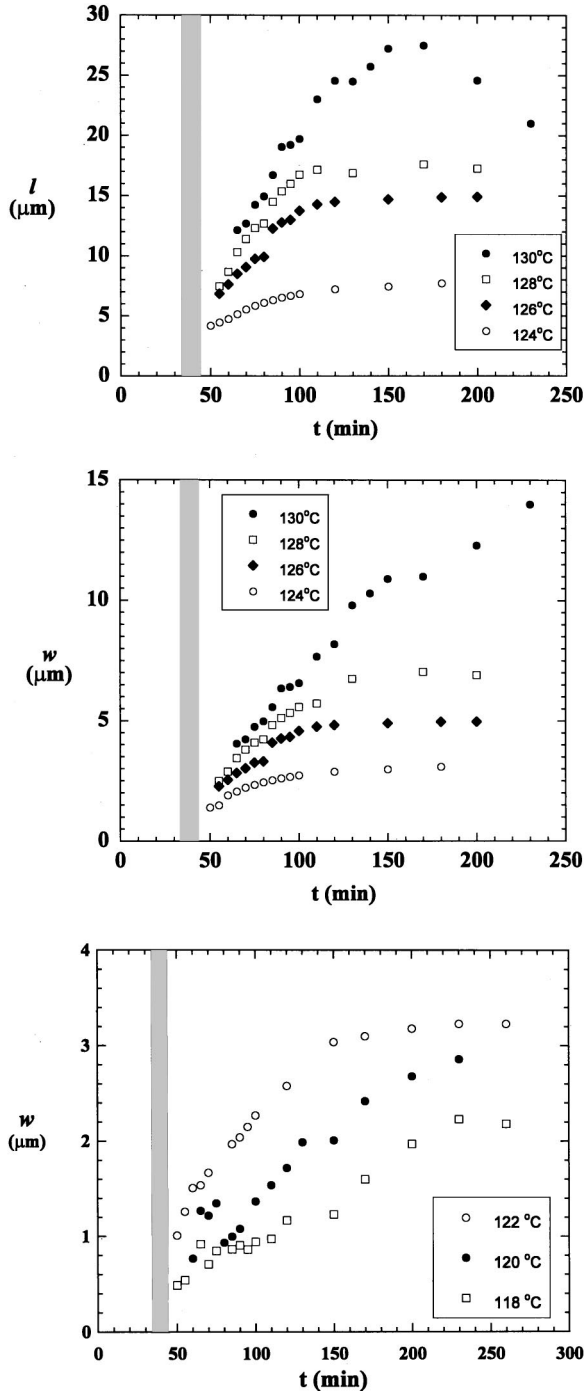

FIG. 6. Time-dependence of grain dimensions l and w at different quench temperatures. Data obtained after shallow quenches are shown in parts (a) and (b). Data obtained after deep quenches, where $l=w$, are shown in part (c). The vertical gray bar indicates the value at t, where the sample temperature reaches the final quench temperature (see Sec. II for details).

[Figs. 6(a) and 6(b)] in spite of the fact that v is more-or-less constant during this time (Fig. 7).

In Fig. 8 we show the time dependence of I_0 obtained at the different quench temperatures. We see that the time dependence of I_0 is similar to that of v; compare Figs. 7 and 8. We find a rapid increase in I_0 at the early times followed by a plateau later (Fig. 8). It is perhaps of interest to note that the plateau values of the I_0 and v decrease by about three orders of magnitude in response to a modest change in

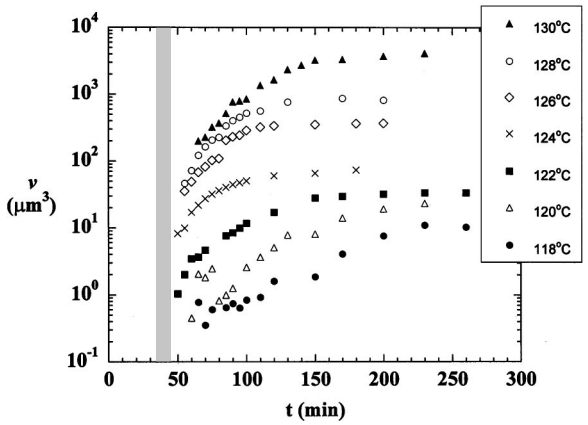

FIG. 7. Time dependence of grain volume, v, at different quench temperatures. The vertical gray bar indicates the value at t, where the sample temperature reaches the final quench temperature.

quench temperature from 130 °C to 118 °C (Figs. 7 and 8).

The classical theory of nucleation and growth is built on the assumption that nuclei of the equilibrium ordered phase grow by consuming the surrounding disordered phase. Since the nuclei are at equilibrium at all times, the order parameter within all of the grains is identical and independent of time. This implies that Δn for the growing nuclei are independent of time. If we assume that ϕ approaches unity at long times, $t=t_L$, where we define t_L to be the time at which each experiment was terminated, then we can use measurements of I_0 and v to estimate ϕ. We define a parameter $f_{\mathrm{nucl}}(t)$ to be equal to the value of I_0/v at any time t, normalized by its value at t_L,

$$f_{\mathrm{nucl}}(t)=\frac{I_0(t)/v(t)}{I_0(t_L)/v(t_L)}. \tag{8}$$

If the disorder-to-order transition is complete at $t=t_L$ or earlier, and if the mechanism of the disorder-to-order transition is classical nucleation and growth, then the grain volume fraction $\phi(t)\equiv f_{\mathrm{nucl}}(t)$; see Eqs. (6) and (8).

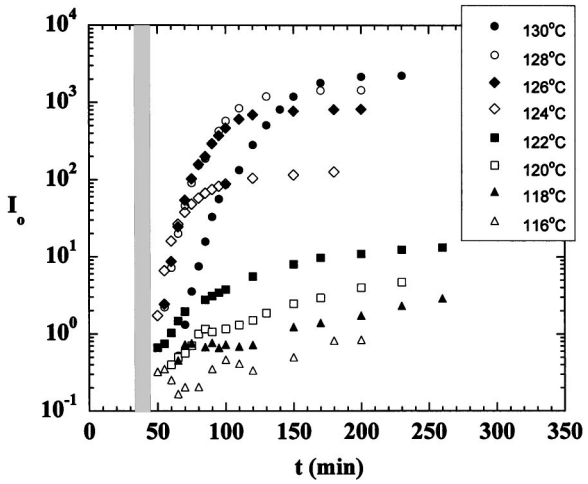

FIG. 8. Time dependence of I_0, the depolarized light scattering intensity as $q\to 0$, at different quench temperatures. The vertical gray bar indicates the value at t, where the sample temperature reaches the final quench temperature.

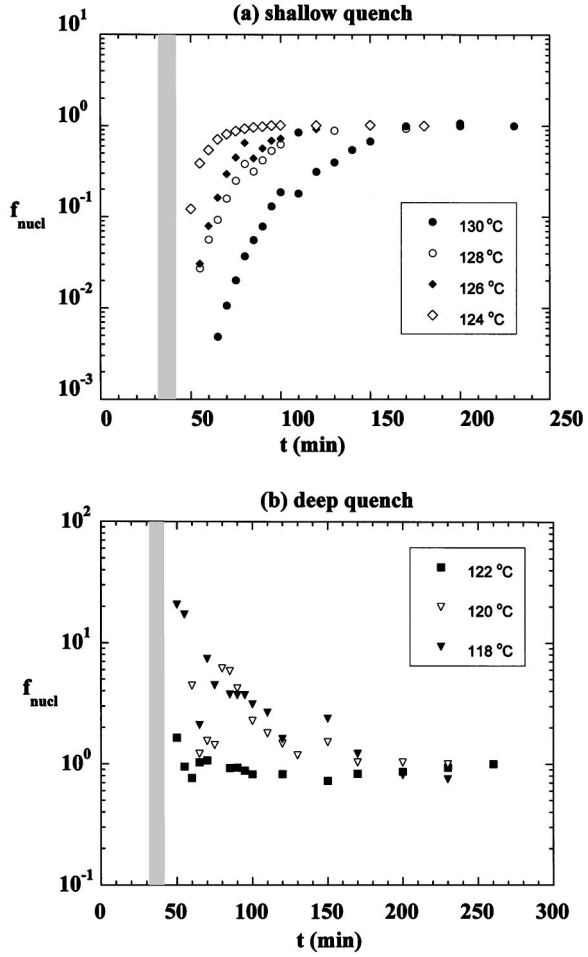

FIG. 9. Time dependence of the factor f_{nucl}, defined by Eq. (8), at different quench temperatures. (a) Shallow quenches, where f_{nucl} can be approximately equated to the volume fraction of the ordered phase, ϕ. (b) Deep quenches, where f_{nucl} cannot be equated to the volume fraction of the ordered phase. The vertical gray bar indicates the value at t, where the sample temperature reaches the final quench temperature.

It is anticipated that classical nucleation theories apply at shallow quenches.[25,26] We thus begin with a discussion of the time dependence of f_{nucl} for shallow quenches (between 130 °C and 124 °C), assuming that $\phi(t) \equiv f_{\mathrm{nucl}}(t)$. The data obtained in the shallow quench depth regime are shown in Fig. 9(a). At early times, the grain volume fraction is small. It increases with time[27] and reaches a plateau that is defined to be unity. The time required for ϕ to reach its asymptotic value can be considerably lower than that required for v to reach its asymptotic value. At 124 °C, for example, clear signs of grain growth can be seen until $t=120$ min (Fig. 7), while $\phi=1$ at $t=70$ min [Fig. 9(a)]. Between $t=70$ and 120 min, at 124 °C, v increases from 30 to 80 $\mu\mathrm{m}^3$ while ϕ remains constant. Grain volume v is determined entirely from the angular dependence of the scattering intensity, while I_0 is unrelated to the angular dependence of the scattering intensity. Thus, at 124 °C between $t=70$ and 120 min, both I_0 and $I(q,\mu)$ change in such a way as to preserve the ratio I_0/v. This behavior is seen during the later stages of grain growth at all temperatures discussed in Fig. 9(a). The observation of a time-independent $\phi \sim I_0/v$ during the later stages provides substantial confirmation of our model because of the fact that the determination of v and I_0 are decoupled. It is also difficult to imagine that this time independent value of ϕ is different from unity. Our observation of grain growth after $\phi \approx 1$ indicates that the defects separating neighboring grains are mobile and grain growth occurs due to annihilation of some of these defects. In the shallow quench depth regime, we can thus identify two stages of grain growth; an early stage where grains grow by consuming the surrounding disordered phase and a late stage where grains grow by defect annihilation. The end of the early stage signals the completion of the disorder-to-order transition. It is seen in Fig. 9(a) that the completion time decreases monotonically with increasing quench depth. At 130 °C, for example, $\phi \approx 1$ at $t=150$ min, while at 124 °C, $\phi \approx 1$ at $t=70$ min. Thus, at 124 °C, ϕ is constant over a considerable portion of the available time window (70–200 min).

An interesting situation arises at a quench temperature of 122 °C, as shown in Fig. 9(b). Under these conditions, f_{nucl}, or equivalently, ϕ, is essentially equal to unity in the entire accessible time window. It is evident that at this quench depth, the disorder-to-order transition is completed before $t=50$ min. Thus the grain growth seen at 122 °C in Figs. 6(c) and 7 is entirely due to defect annihilation, and the time required for completion of the disorder-to-order transition is below our resolution limit.

The time dependence of f_{nucl} for deeper quenches (120 °C and 118 °C) is also shown in Fig. 9(b). A comparison of the data in Figs. 9(a) and 9(b) provides the first indications of a qualitative difference between shallow and deep quenches. During shallow quenches [Fig. 9(a)], f_{nucl} increases with time, while during deep quenches [Fig. 9(b)], f_{nucl} decreases with time. At the border between shallow and deep quenches f_{nucl} is independent of time [$T=122$ °C in Fig. 9(b)]. It is clear that in the deep quench regime, $\phi(t)$ is not equal to $f_{\mathrm{nucl}}(t)$ because f_{nucl} is significantly larger than unity at early times [Fig. 9(b)]. This means a breakdown in the underlying assumptions used to equate ϕ and f_{nucl}.

It is conceivable that grains formed during deep quenches do not have the same Δn. This necessarily implies that some (or all) of the grains formed during deep quenches are not at equilibrium. The decrease in f_{nucl} with time may then be attributed to a reduction in the Δn polydispersity, as the grains attempt to approach equilibrium. It is also possible that deep quenches lead to a broad distribution of grain sizes. This polydispersity effect ($f_{\mathrm{nucl}}>1$) is clearly seen at 120 °C and 118 °C but hints of such behavior are contained in the data at 122 °C [Fig. 9(b)]. A more complete description of the polydisperse grain structure obtained during deep quenches will require the development of more sophisticated models than those used in this paper.

In Fig. 10 we plot the final characteristic lengths of the grains obtained at $t=t_L$. We find a sharp distinction between the grains formed after shallow quenches $T>123$ °C and grains formed after deep quenches $T<123$ °C. In the shallow quench regime we obtain anisotropic grains ($l \neq w$) that are large while in the large quench regime we find isotropic grains ($l=w$) that are small.

Anisotropic grains are expected to form during the early stages of the disorder-to-order transition due to the anisot-

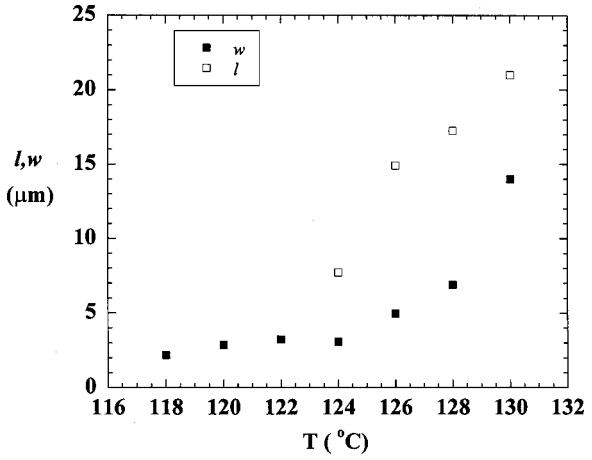

FIG. 10. The dependence of the final grain parameters l and w at $t=t_f$ on quench temperature T.

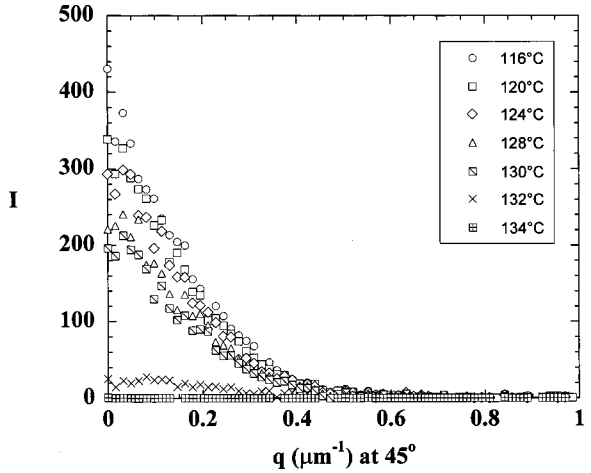

FIG. 11. Depolarized scattering intensity, I, vs scattering vector, q, along the $\mu=45°$ direction. Equilibrated ordered grains were grown by quenching to 124 °C. The sample was then cooled to 116 °C and studied as a function of increasing temperature.

ropy of the hexagonal microstructure.[10] The interfacial tension between the ordered phase and the surrounding disordered phase depends on the orientation of the interface relative to the optic axis and this will induce the formation of ellipsoidal grains. The Wulff construction[2] can be used to determine the shape of the ordered grains that would grow if the ordering process were carried out at infinitesimal quench depth. One thus expects anisotropic grains to emerge during the early stages of shallow quenches when grain growth is slow and the grains are well separated from their neighbors. This is consistent with our observations at shallow quench depths, see early time data in Figs. 6(a) and 6(b). However, after the disorder-to-order transition is complete, the ordered grains are no longer in contact with the disordered phase and the driving forces that led to the formation of ellipsoidal grains are no longer operative. Decreasing Gibbs energy in a fully ordered sample requires reducing defect density. One mechanism of accomplishing this is by reducing the anisotropy of grains, i.e., reducing l/w, at constant grain volume. The decrease in l with increasing time observed during the late stages of ordering at 130 °C [Fig. 6(a)] is a spontaneous process because grain volume remains constant during this time (see Fig. 7). At all other quench temperatures, grains grow irreversibly, i.e., l and w increase monotonically with time [Figs. 6(a)–6(c)].

We conclude that kinetic factors dominate grain growth in the deep quench regime because isotropic grains were obtained during all stages of order formation [Fig. 6(c)]. We conducted additional experiments to study the polydisperse and nonequilibrium character of the grain structure formed during deep quenches. The results of these experiments are described below.

V. EFFECT OF TEMPERATURE ON EQUILIBRIUM ORDER PARAMETER

An SI(20-6) sample was subjected to a quench to 124 °C and held there until $t=180$ min as discussed in Sec. IV. This is the first step of the experiment (step 1). The sample is filled with equilibrated grains at the end of this step [see 124 °C data in Fig. 9(a)]. The sample temperature was then reduced to 116 °C and the depolarized light scattering signal was studied as a function of increasing temperature. We waited for 20 min at each temperature to ensure thermal equilibration of the sample and then measured the depolarized light scattering profile. We refer to this as a multistep quench experiment to contrast it from the direct quench experiments described in the preceding section. The resulting scattering profiles $[I(q,\mu=45°)]$ at selected temperatures are shown in Fig. 11. We obtained anisotropic scattering patterns at all of the temperatures and we thus used Eqs. (2)–(5) to analyze the data. The anisotropy in scattering was not large so we do not show $[I(q,\mu=0°)]$. We assume that $\phi=1$ when the sample temperature is below 133 °C ($T_{\mathrm{ODT}}=133$ °C). We obtain v from the angular dependence of $I(q)$ and estimate Δn using the relationship $|\Delta n|\sim(I_0/v)^{1/2}$. We define a normalized refractive index difference $|\Delta n|_{\mathrm{equil}}$ as follows:

$$|\Delta n|_{\mathrm{equil}}=\frac{|\Delta n|}{|\Delta n|_{T=124C}}=\sqrt{\frac{I_0/v}{(I_0/v)_{124Cstep1}}}\quad\text{(multistep quenches)},\qquad(9)$$

where we use the subscript ''equil'' to indicate that the relative $|\Delta n|$ value that we obtain is from a sample with equilibrated grains, and $(I_0/v)_{124Cstep1}$ is the value of I_0/v after the first step of our multistep quench. We cannot compute the absolute value of $|\Delta n|$ because we have not determined the proportionality constant between $|\Delta n|$ and $(I_0/v)^{1/2}$. We have normalized $|\Delta n|$ by its value at 124 °C, the temperature at which the grains were grown. The solid symbols in Fig. 12 represent the temperature dependence of $|\Delta n|_{\mathrm{equil}}$. It is evident that $|\Delta n|_{\mathrm{equil}}$ is a weak function of temperature in the range $116\,°\mathrm{C}\leqslant T\leqslant 130\,°\mathrm{C}$. We find a dramatic decrease in the scattered intensity when the temperature is changed from 130 to 132 °C (Fig. 11). We are not sure about the state of the sample at 132 °C after a multistep quench. Perhaps the sample is partially disordered. We note that 132 °C is precariously close to T_{ODT} (133 ± 1 °C), and factors such as

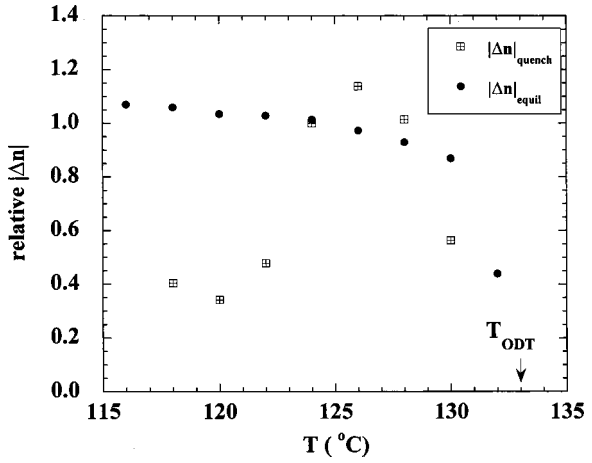

FIG. 12. The temperature dependence of the average birefringence within grains for quenched and equilibrated samples; $|\Delta n|_{\text{equil}}$ defined by Eq. (9) and $|\Delta n|_{\text{quench}}$ defined by Eq. (10).

polydispersity in chain length and limited control over thermal history may affect our results.[28] We therefore do not attempt to explain the magnitude of the measured value of $|\Delta n|_{\text{equil}}$ at 132 °C.

It is evident that the grain structure obtained from a direct quench to a given temperature (Fig. 2) is dramatically different from the grain structure obtained after a multistep quench to the same temperature (Fig. 11). For example, at 128 °C, the direct quench leads to a grain structure with a much larger value of I_0 [$I_0=1450$; see Fig. 2(c)] than that obtained from a multistep quench ($I_0=220$; see Fig. 11). In contrast, at 120 °C, the direct quench leads to a grain structure with a much smaller value of I_0 [$I_0=14$; see Fig. 2(g)] than that obtained from a multistep quench ($I_0=320$; see Fig. 11). Some of these differences are due to the dependence of grain size on quenching history. This is not surprising because the grain structure is completely determined by the irreversible aspects of the disorder-to-order phase transition, and the products of irreversible processes are often path dependent. However, all of the changes in I_0 cannot be accounted by changes in grain volume alone and there are additional effects that must be related to the internal structure within the grains which affect $|\Delta n|$. To focus on these effects, we define, $|\Delta n|_{\text{quench}}$, the relative value of $|\Delta n|$ obtained from a direct quench experiment again normalized to its value at 124 °C,

$$|\Delta n|_{\text{quench}} = \sqrt{\frac{I_0(t_F)/v(t_F)}{(I_0(t_F)/v(t_F))_{T=124C}}} \quad \text{(direct quenches)}. \tag{10}$$

The results of this exercise are shown by squares in Fig. 12. The value of $I_0(t_F)/v_F$ used in the normalization of $|\Delta n|_{\text{quench}}$ was 1.309, while the I_0/v value used in the normalization of $|\Delta n|_{\text{equil}}$ was 1.284. The difference between these numbers indicates the extent to which the grain structure in different samples subjected to the same thermal history was reproducible.

Figure 12 enables a comparison between the average order parameter of the grains obtained from a direct quench ($|\Delta n|_{\text{quench}}$) with that of equilibrated grains ($|\Delta n|_{\text{equil}}$). At a quench temperature of 132 °C, we do not see any signs of ordering [Fig. 2(a)] so $|\Delta n|_{\text{quench}}$ could not be measured at this temperature. At 130 °C, $|\Delta n|_{\text{quench}}$ is significantly less than $|\Delta n|_{\text{equil}}$. We thus observe severe hysteresis in the 130–133 °C temperature range. It is evident that our experimental protocol is unable to establish the nature of the equilibrium ordered state in the 130–133 °C range. Such hysteresis is inevitable near the phase boundary of systems undergoing a first-order phase transition. At temperatures between 128 and 124 °C, however, there is near-quantitative agreement between $|\Delta n|_{\text{quench}}$ and $|\Delta n|_{\text{equil}}$. This agreement is obtained in spite of the large difference in the scattering profiles obtained after direct and multistep quenches. We conclude that grains formed by direct quenches to 128 °C, 126 °C, and 124 °C are at equilibrium. By definition, there should be no polydispersity of Δn in this temperature range. At 122 °C, 120 °C, and 118 °C, however, $|\Delta n|_{\text{quench}}$ is significantly smaller than $|\Delta n|_{\text{equil}}$, indicating that the grains formed in the deep quench regime are out of equilibrium (Fig. 12).

The data discussed in Sec. IV showed qualitative differences in grain size obtained in the shallow and deep quench regimes (Figs. 9 and 10). The data in this section confirms that the internal structure of the grains formed in the shallow and deep quench regimes is also qualitatively different.

VI. RHEOLOGY

The objective of this section is to obtain the characteristic relaxation time in SI(20-6) melts from rheological measurements. We restrict our attention to the disordered state where the relationship between relaxation processes and rheological measurements is reasonably well established. The frequency (ω) dependence of the real and imaginary parts of the shear stress relaxation modulus, G' and G'', respectively, were measured as a function of decreasing temperature from 145 to 133 °C. The data obtained at 133 °C are shown in Fig. 13(a). Conventional time-temperature superposition[29] was used to shift data obtained at higher temperatures and the shifted data are also shown in Fig. 13(a). The temperature dependence of a_T, the shift factors used to collapse the data, are given in Fig. 13(b). The $G''(\omega)$ data exhibit simple behavior. Approximate liquidlike behavior $G'' \sim \omega^1$ is seen in the low frequency limit and time-temperature superposition leads to a reasonable collapse of the data [Fig. 13(a)]. In contrast, we see some complexity in the $G'(\omega)$ data. Time-temperature superposition does not lead to perfect collapse at low frequencies. In addition, power law fits through the low frequency G' data yield an exponent 1.7 at all temperatures, instead of the expected value of 2. Similar results were obtained by Jin and Lodge in their comprehensive study of the rheology of block copolymer solutions.[30] It is believed that this complexity is due to the presence of concentration fluctuations in disordered block copolymer systems. The amplitude of the fluctuations is temperature dependent and this causes failure of time–temperature superposition. Following Jin and Lodge, we estimate the characteristic time scale for relaxation of concentration fluctuations, τ_{fluc}, by a power law extrapolation of the low frequency G' and G'' data, and locating ω_{int} the frequency at the intersection point of the power law lines. Note

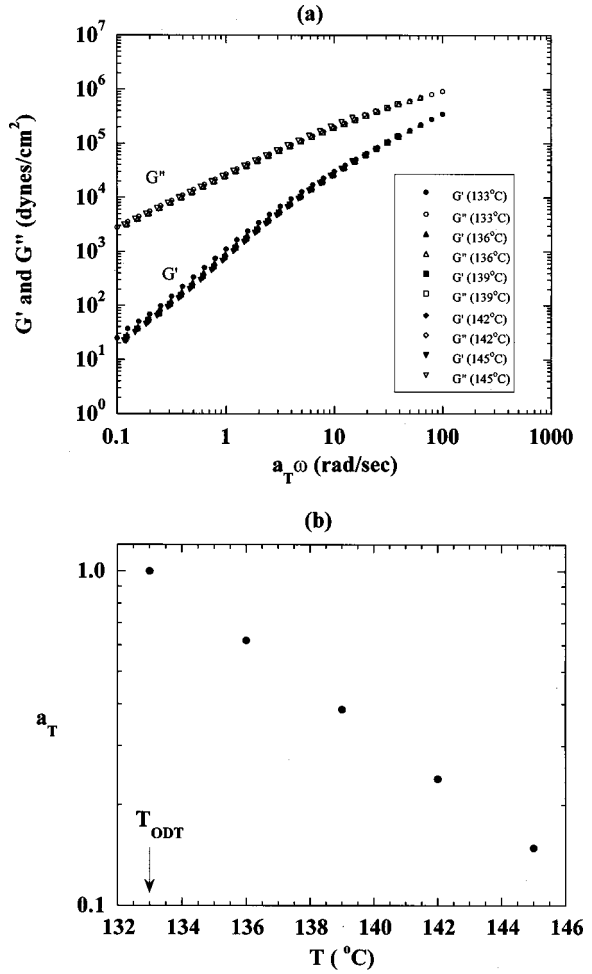

FIG. 13. (a) The frequency (ω) dependence of the real and imaginary parts of the stress relaxation modulus, G' and G'', respectively, after time–temperature superposition, at a reference temperature of 133 °C. (b) The temperature dependence of the shift factors, a_T, used to obtain the superposition shown in part (a).

that ω_{int} is temperature dependent due to the lack of perfect time–temperature superposition; see Fig. 13(a). We take

$$\tau_{\text{fluc}} = \frac{a_T}{\omega_{\text{int}}}. \tag{11}$$

The temperature dependencies of ω_{int} and τ_{fluc} are given in Table I.

VII. SMALL ANGLE NEUTRON SCATTERING

The q dependence of the coherent SANS intensity I_{SANS} from SI(20-6) at selected temperatures is shown in Fig. 14. The sample was first disordered and studied as a function of decreasing temperature. A scattering peak is seen at $q = q_{\text{peak}} \approx 0.37\,\text{nm}^{-1}$ regardless of temperature. The location of the scattering peak is in agreement with literature.[31,32] At temperatures $\geqslant 135\,°\text{C}$, the scattering peak indicates the length scale of disordered concentration fluctuations. At temperatures $\leqslant 131\,°\text{C}$, the scattering peak gives the average lattice constant of the hexagonal phase, $d = 2\pi/0.37 = 17.0\,\text{nm}$. There is no sharp distinction between SANS data obtained from the disordered and ordered state. This is consistent with previously published literature, e.g., Ref. 21.

TABLE I. Temperature dependence of the rheological properties of disordered SI(20-6).

T (°C)	a_T	ω_{int} (rad/s)	τ_{fluc} (s)
133	1.000	111.00	0.0090
136	0.642	132.50	0.0049
139	0.413	158.50	0.0026
142	0.268	171.00	0.0016
145	0.177	185.00	0.0010

VIII. MECHANISMS OF GRAIN FORMATION

We now combine the results of depolarized light scattering, rheology, and SANS, to identify the factors that control grain formation in SI(20-6) melts. In particular we would like to know the reason for the qualitative difference in grains formed by quenches above and below 123 °C. One possible reason for this difference is a mechanistic change in the disorder-to-order phase transition at 123 °C. The mean-field theory of block copolymers predicts the presence of a spinodal at temperatures just below the stability limit of the hexagonal phase.[31] If the spinodal for our system were located at 123 °C, then above 123 °C we would obtain conventional nucleation and growth while below 123 °C we would obtain spinodal decomposition. It is therefore possible that the complex grain structures observed below 123 °C are a product of spinodal decomposition. The presence of a spinodal is indicated by a divergence in the disordered state structure factor.[31] In Fig. 15 we plot $1/I_{\text{peak}}$ vs $1/T$, the conventional plot for locating the spinodal within the mean-field approximation. The data obtained in the disordered state were extrapolated to the point where $1/I_{\text{peak}} \rightarrow 0$. As shown in Fig. 15, the spinodal obtained by this procedure is located at 88 °C. Our data rule out the possibility of a divergent peak intensity at 123 °C ($1/T = 0.0025\ K^{-1}$). Thus, the reason for the complex grain structure obtained below 123 °C cannot be

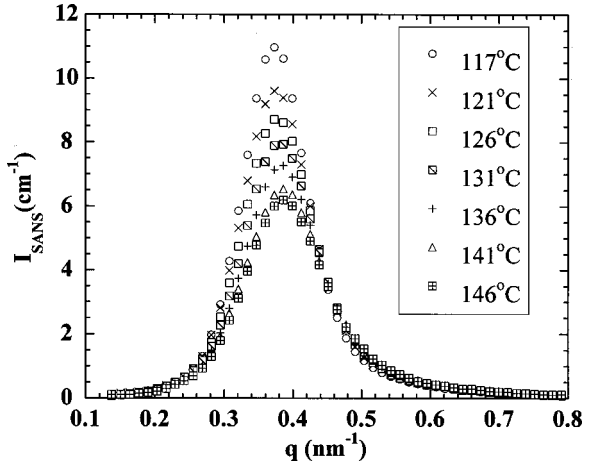

FIG. 14. SANS intensity, I_{SANS} vs scattering vector q at selected temperatures.

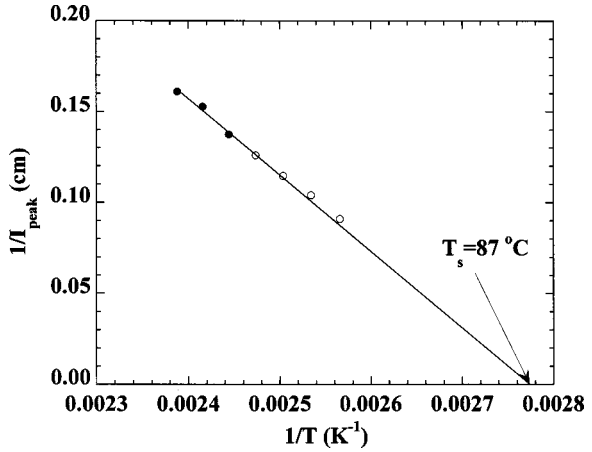

FIG. 15. A plot of $1/I_{peak}$ the SANS intensity at the peak vs the reciprocal of absolute temperature, $1/T$. Filled circles, disordered state. Open symbols, ordered state. A linear fit through the disordered state data was used to estimate the spinodal temperature, T_s.

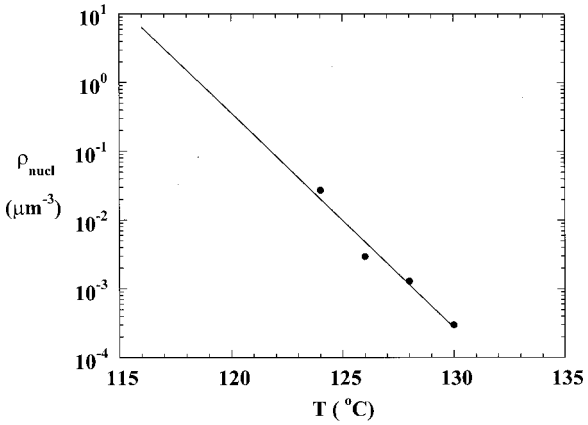

FIG. 17. The nucleation density, ρ_{nucl}, vs temperature. The line is used to extrapolate the measured trends to the temperature range ρ_{nucl} could not be measured directly.

due to a change in the phase transition mechanism. We therefore consider the possibility that our observations are due to kinetic reasons.

Our determination of $\phi(t)$ in Fig. 9(a) enables the determination of the time required to complete the disorder-to-order transition. This time, which we call τ_{order}, is defined to be the earliest time at which $\phi > 0.9$ was recorded minus 37 min (the average time required to quench the sample). Our error in τ_{order} due to the finite time required to quench the sample is ± 5 min. At 124 °C, for example, $\phi > 0.9$ at $t \geqslant 70$ min, and τ_{order} is thus 34 ± 5 min. We determined τ_{order} in the available temperature window (130 °C to 124 °C) and our results are shown in Fig. 16. Also shown in Fig. 16 is the temperature dependence of τ_{fluc}, the characteristic time scale for relaxation of concentration fluctuations in the disordered state, taken from Table I. To a good approximation, both time scales exhibit exponential dependencies on temperature. The lines in Fig. 16 are least squares fits through the data.

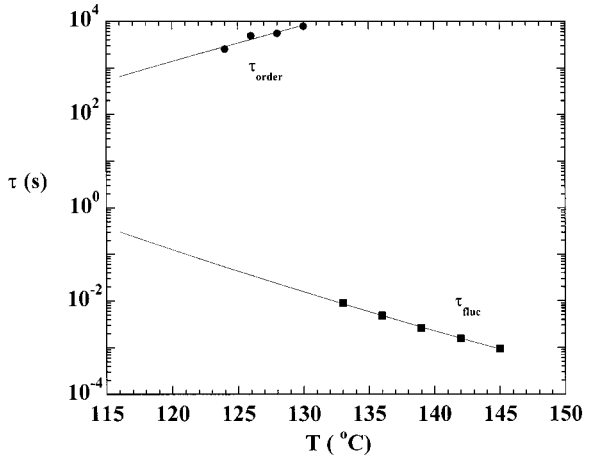

FIG. 16. The temperature dependence of relevant time scales. Circles, time required to complete the disorder-to-order transition, τ_{order}. Squares, intrinsic time scale for fluctuation relaxation, τ_{fluc}. The lines are used to extrapolate the measured trends to the temperature range where τ_{order} and τ_{fluc} could not be measured directly.

The observed exponential temperature dependencies of τ_{order} and τ_{fluc} on temperature are not surprising. The exponential temperature dependence of the relaxation time is characteristic of fluids at temperatures that are well above the glass transition temperature. The exponential decrease of τ_{order} with increasing quench depth, indicates that the order formation in our system are dominated by thermodynamic driving forces which become stronger with quench depth. We could not measure τ_{fluc} at temperatures below 133 °C because of the formation of the ordered phase, which has completely different rheological characteristics. Similarly, we could not measure τ_{order} at temperatures below 124 °C because the time required to complete the disorder-to-order transition was smaller than the time required to quench the sample. In the range where direct measurements are not possible, we estimate τ_{order} and τ_{fluc} using extrapolations of the exponential fits, i.e., the lines in Fig. 16.

The grain structure at completion ($t = \tau_{order} + 36$ min) gives an estimate the density of nuclei that are formed during the disorder-to-order transition. If we assume that each nucleus gives rise to one grain at completion, then the number of nuclei per unit volume, $\rho_{nucl} = 1/v(t = \tau_{order})$. Some justification for this assumption comes from the fact that grain growth by defect annihilation is much slower than grain growth by consumption of the disordered phase (Fig. 7). The ρ_{nucl} values that we compute is a lower bound on the true nucleation density because some defect annihilation must take place before completion of the disorder-to-order transition. In Fig. 17 we plot ρ_{nucl} vs quench temperature T. It is evident that to a good approximation ρ_{nucl} is an exponential function of temperature. The line in Fig. 17 is the least squares exponential fit through the data. As was the case with τ_{fluc} and τ_{order}, extrapolation of the exponential fits were used to estimate ρ_{nucl} at temperatures where direct measurements were not possible. The complimentary trends observed in the temperature dependencies of τ_{order} and ρ_{nucl} indicate that the rapid completion times observed with increasing quench depths are due to increasing nucleation densities and not due to rapid grain growth kinetics.

The formation of long range order requires a certain

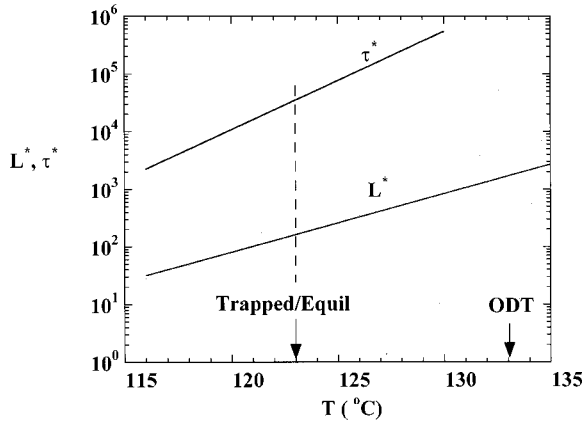

FIG. 18. The temperature dependence of dimensionless parameters L^*, the ratio of the characteristic distance between nuclei and the characteristic length of the ordered phase, and τ^*, the ratio of the time required to form the ordered phase to the characteristic time for relaxation of concentration fluctuations.

amount of space and time. The space available for a given nucleus to grow is limited by the neighboring nuclei. The average distance between neighboring nuclei L_{nucl}, given by $L_{\mathrm{nucl}}=\sqrt[3]{v(t=\tau_{\mathrm{order}})}$, is thus a measure of the space available for order formation. The time available for order formation is τ_{order}. We define a dimensionless time scale τ^*,

$$\tau^* = \frac{\tau_{\mathrm{order}}}{\tau_{\mathrm{fluc}}}, \tag{12}$$

and a dimensionless length scale L^*,

$$L^* = \frac{L_{\mathrm{nucl}}}{d}. \tag{13}$$

It is clear that L^* and τ^* must be greater than unity for classical nucleation and growth kinetics to be observed, because d and τ_{fluc} are obvious lower bounds for the space and time required for nucleation. However, it is conceivable that order formation is a collective phenomenon, requiring the concerted rearrangement of several molecules. If this is true then L^* and τ^* must be significantly greater than unity for classical nucleation and growth kinetics to be observed. In Fig. 18 we plot L^* and τ^* as a function of temperature. At 123 °C, the temperature at which we observe a change in grain structure from equilibrated grains to kinetically trapped grains, we find that $L^*=10^2$ while $\tau^*=2\times10^4$, i.e., $L^* \ll \tau^*$. Since L^* is significantly smaller than τ^*, not only at 123 °C but through the entire experimental temperature window (Fig. 18), we conclude that the primary limitation that prevents equilibration in the deep quench regime is the lack of space. We also conclude that temporal constraints due to rapid ordering kinetics in the deep quench regime are not responsible for the kinetic trapping. The result that $L^*=100$ at 123 °C, suggests that order formation in our system is a collective phenomenon that involves concerted motion of about 100 chains. If space for such concerted motion is not available, the resulting ordered phase falls out of equilibrium.

IX. CONCLUDING REMARKS

Grain growth in SI(20-6) melts was studied by time-resolved depolarized light scattering after a quiescent quench from the disordered to the ordered state. The sample exhibits an order–disorder transition at 133 ± 1 °C. At quench temperatures above 123 °C, we observed grain growth kinetics that were consistent with classical nucleation and growth. At quench temperatures below 123 °C, however, we obtained small, highly disorganized grains that were out of equilibrium. We show that the abrupt change in grains structure at 123 °C is due to spatial constraints set by very high nucleation densities.

Whether or not we should conclude that the disorder-to-order transition is complete in our experimental window in the deep quench regime is an interesting question. The phase transition is far from complete if we define the final product to be the equilibrium phase. On the other hand, if we accept the poorly ordered phase as the final product, then the phase transition is completed rather quickly (see Fig. 16). The formation of the equilibrium grain structure in the deep quench regime would be indicated by values of f_{nucl} that are about an order of magnitude larger than those obtained at the end of our experiments. This would require a substantial increase in f_{nucl} with time. On experimental time scales, however, we only observe a decrease in f_{nucl} with time in the deep quench regime [Fig. 9(b)]. The time scale on which the kinetically trapped nonequilibrium phase formed at deep quenches will transform into the equilibrium phase is completely outside our experimental window. This fact, in conjunction with the structural polydispersity that we find in the deep quench regime, are reminiscent of glassy systems. In the deep quench regime, however, the polystyrene microphase about 40 °C above its glass transition temperature (T_g). The stability of the kinetically trapped state thus cannot be attributed to molecular sluggishness encountered near the conventional T_g. It appears that the poorly ordered, polydisperse grains that fill our sample during deep quenches do not have access to pathways for approaching equilibrium.

Liquid crystalline systems are generally characterized by low defect densities, due to high mobility in the liquid directions. In low molecular weight liquid crystals, closely spaced defects annihilate rapidly[33] resulting in very large grains and textures that have become the standard signatures[2,3] of these systems. Similar textures have been seen in block copolymer systems with low defect densities.[34,35] In deeply quenched SI(20-6) melts, however, we have demonstrated the opposite tendency, namely the ability to trap high defect density states that are far from equilibrium.

In a previous paper[13] we studied the kinetics of order formation in another molten block copolymer, SI(4-13) where the numbers in the brackets refer to the molar masses of the polystyrene and polysioprene blocks, respectively, in kg/mol. T_{ODT} for this sample was 59 ± 1 °C. The composition of SI(4-13) and SI(20-6) are similar except for the fact that polystyrene is the minor component in the former and polyisoprene is the minor component in the latter. The grain growth characteristics of SI(4-13) and SI(20-6) at shallow quench depths are virtually identical; compare data in Refs. 10–13 to present paper. In SI(4-13) we found an abrupt

change in ordering kinetics at a quench temperature of 53 °C; the grain structure formed during the early stages below 53 °C was highly disorganized. There are thus some similarities in the deep quench data obtained in SI(4-13) and SI(20-6) melts.

There are, however, three important differences between the results obtained from SI(4-13) and SI(20-6).

(1) The SANS profiles from SI(4-13) indicated a divergence of I_{peak} in the vicinity of 53 °C. We did not mention this in Ref. 13 but data presented in a previous paper[21] shows this effect. We now recognize this divergence to be a stringent requirement for postulating the presence of a buried spinodal.

(2) At all of the quench temperatures and at all times we found that f_{nucl} in SI(4-13) was less than unity, and it monotonically increased with time. There was thus no evidence for the formation of nonequilibrium grain structure in SI(4-13).

(3) The disorganized grains formed during the early stages in SI(4-13) transform into the equilibrium ordered phase on experimental time scales.

Point (1) is consistent with the notion that the poorly organized grains formed during the early stages during deep quenches of SI(4-13) are due to spinodal decomposition. Points (2) and (3) indicate the lack of kinetic trapping in SI(4-13). The conclusion of our previous study,[13] that the abrupt change in the grains structure in SI(4-13) was due to a change in the phase transition mechanism from nucleation and growth to spinodal decomposition, thus appears robust.

Based on our studies thus far, we conclude that a disorganized grain structure formed during the early stages of the disorder-to-order transition in block copolymer melts can be due to many reasons. In some systems like SI(4-13) it appears to be the consequence of an underlying spinodal. In other systems like SI(20-6) it appears to be a consequence of spatial constraints set up by very large nucleation densities. It is possible that in other systems, temporal constraints will result in the formation of a disorganized grain structure. The answer to the question first raised by Hajduk *et al.*,[36] whether the grains structure in block copolymers is controlled by thermodynamic or kinetic factors, appears to be system dependent.

Some theories have addressed the role of underlying thermodynamic features such as spinodals on the formation and disappearance of nonequilibrium structures.[37,38] Recent simulations[39] suggest that hydrodynamics may play a key role in the annealing of nonequilibrium structures formed during the early stages. Other theories assume that order formation occurs by classical nucleation and growth.[40,41] Our experiments indicate that nucleation density plays an essential role in determining the grain structure in some block copolymers. We are not aware of testable theoretical predictions for the variation of nucleation density with quench depth in block copolymer melts. We are also not aware of any predictions of nucleation densities required for kinetic trapping. We hope that our work will motivate the development of more complete theories on the kinetics of the disorder to order transition in block copolymers.

ACKNOWLEDGMENTS

We thank Amy Lefebvre and Boualem Hammouda for their help with the SANS experiments, and Nikolay Vladimirov for conducting the DSC measurements. Financial support provided by the National Science Foundation (DMR-9901951, DMR-9975592), and the Dreyfus Foundation, is gratefully acknowledged. The SANS instrument at NIST is supported by the National Science Foundation (DMR-9986442) (Ref. 42).

[1] D. A. Porter and K. E. Easterling, *Phase Transformations in Metals and Alloys* (Chapman and Hall, New York, 1992).
[2] P. M. Chaikin and T. C. Lubensky, *Principles of Condensed Matter Physics* (Cambridge University Press, New York, 1995).
[3] P. G. De Gennes and J. Prost, *The Physics of Liquid Crystals* (Oxford, New York, 1993).
[4] C. A. Angell, in *The Physics of Complex Systems*, edited by F. Mallamace and H. E. Stanley (IOS, New York, 1977), p. 571.
[5] P. G. Debenetti, *Metastable Liquids* (Princeton University Press, Princeton, New Jersey, 1996).
[6] F. S. Bates and G. H. Fredrickson, Annu. Rev. Phys. Chem. **41**, 525 (1990).
[7] N. P. Balsara, B. A. Garetz, and H. J. Dai, Macromolecules **25**, 6072 (1992).
[8] B. A. Garetz, M. C. Newstein, H. J. Dai, S. V. Jonnalagadda, and N. P. Balsara, Macromolecules **26**, 3151 (1993).
[9] B. A. Garetz, N. P. Balsara, H. J. Dai, Z. Wang, M. C. Newstein, and B. Majumdar, Macromolecules **28**, 4587 (1996).
[10] H. J. Dai, N. P. Balsara, B. A. Garetz, and M. C. Newstein, Phys. Rev. Lett. **77**, 3677 (1996).
[11] M. C. Newstein, B. A. Garetz, N. P. Balsara, M. Y. Chang, and H. J. Dai, Macromolecules **31**, 64 (1998).
[12] N. P. Balsara, B. A. Garetz, M. Y. Chang, H. J. Dai, M. C. Newstein, J. L. Goveas, R. Krishnamoorti, and S. Rai, Macromolecules **31**, 5309 (1998).
[13] N. P. Balsara, B. A. Garetz, M. C. Newstein, B. J. Bauer, and T. J. Prosa, Macromolecules **31**, 7668 (1998).
[14] H. Wang, M. C. Newstein, M. Y. Chang, N. P. Balsara, and B. A. Garetz, Macromolecules **33**, 3719 (2000).
[15] S. P. Gido, J. Gunther, E. L. Thomas, and D. Hoffman, Macromolecules **27**, 4506 (1993).
[16] S. P. Gido and E. L. Thomas, Macromolecules **27**, 6137 (1994).
[17] E. Huang, P. Mansky, T. P. Russell, C. Harrison, P. M. Chakin, R. A. Register, C. J. Hawker, and J. Mays, Macromolecules **33**, 80 (2000).
[18] C. Harrison, P. M. Chaikin, D. A. Huse, R. A. Register, D. H. Adamson, A. Daniel, E. Huang, P. Mansky, T. P. Russell, C. J. Hawker, D. A. Egolf, I. V. Melnikov, and E. Bodenschatz, Macromolecules **22**, 857 (2000).
[19] J. Hahm, W. A. Lopes, H. M. Jaeger, and S. J. Sibener, J. Chem. Phys. **109**, 10111 (1998).
[20] R. T. Myers, R. E. Cohen, and A. Bellare, Macromolecules **32**, 2706 (1999).
[21] C. C. Lin, S. V. Jonnalagadda, P. K. Kesani, H. J. Dai, and N. P. Balsara, Macromolecules **27**, 7769 (1994).
[22] K. R. Amundson, E. Helfand, S. S. Patel, X. Quan, and S. S. Smith, Macromolecules **25**, 1935 (1992).
[23] N. P. Balsara, D. Perahia, C. R. Safinya, M. Tirrell, and T. P. Lodge, Macromolecules **25**, 6072 (1992).
[24] F. S. Bates, M. F. Schulz, A. K. Khandpur, S. Forster, J. H. Rosedale, K. Almdal, and K. Mortensen, Faraday Discuss. **98**, 7 (1994).
[25] J. W. Cahn and J. E. Hilliard, J. Chem. Phys. **31**, 688 (1959).
[26] K. Binder, Physica A **213**, 118 (1995).
[27] A discontinuity in the data is seen at $t \approx 100$ min at $T = 130$ °C in Fig. 9(a). Similar discontinuities are seen at other temperatures. This discontinuity occurs at the time at which the neutral density filter was introduced. It indicates that our correction procedure, based entirely on the monitor reading (see Sec. II), is somewhat inadequate. Other problems arise due to the steep changes in scattering intensity with scattering angle [see Figs. 2(b)–2(e)] and the limited resolution of the CCD camera. We made several attempts to eliminate this discontinuity but were unsuccessful.
[28] T. Koga, T. Koga, and T. Hashimoto, J. Chem. Phys. **110**, 11076 (1999).
[29] J. D. Ferry, *Viscoelastic Properties of Polymers* (Wiley, New York, 1980).
[30] X. Jin and T. P. Lodge, Rheol. Acta **36**, 229 (1997).

[31] L. Leibler, Macromolecules **13**, 1602 (1980).
[32] Equation (15) in Ref. 21.
[33] R. Snyder, A. N. Pargellis, P. A. Graham, and B. Yurke, Phys. Rev. A **45**, 2169 (1992).
[34] J. C. Wittmann, B. Lotz, F. Candau, and A. J. Kovacs, J. Polym. Sci., Polym. Phys. Ed. **20**, 1341 (1982).
[35] W. Wang, and T. Hashimoto, Macromolecules **32**, 3163 (1999).
[36] D. A. Hajduk, T. Tepe, H. Takenouchi, M. Tirrell, F. S. Bates, K. Almdal, and K. Mortensen, J. Chem. Phys. **108**, 326 (1998).
[37] S. Qi and Z. G. Wang, Phys. Rev. Lett. **76**, 1679 (1996).
[38] S. Qi and Z. G. Wang, J. Chem. Phys. **111**, 10681 (1999).
[39] R. D. Groot, T. J. Madden, and D. J. Tildesley, J. Chem. Phys. **110**, 9739 (1999).
[40] G. H. Fredrickson and K. Binder, J. Chem. Phys. **91**, 7265 (1989).
[41] J. L. Goveas and S. T. Milner, Macromolecules **30**, 2605 (1997).
[42] Certain equipment and instruments or materials are identified in this paper in order to adequately specify the experimental details. Such identification does not imply recommendation by the National Institute of Standards and Technology, nor does it imply the materials are necessarily the best available for the purpose.